

Energy densities and equilibration in heavy ion collisions at $\sqrt{s_{NN}} = 200$ GeV with the quark-gluon string model

J. Bleibel, G. Baur, Amand Faessler, C. Fuchs

*Institute for Theoretical Physics, University of Tübingen, Auf der Morgenstelle 14,
D-72076 Tübingen, Germany*

Abstract

We study thermodynamic characteristics of ultra-relativistic Au+Au collisions at RHIC energy $\sqrt{s_{NN}} = 200$ GeV within the framework of a microscopic transport model, namely the quark-gluon string model (QGSM). The temporal evolution of the local energy density, transverse and longitudinal pressure and equilibration times are considered. In contrast to complete equilibration which is even in central reactions hardly achieved, pre-equilibrium stages with energy densities well above the critical energy density predicted by lattice QCD are established at short time scales. Corresponding energy density profiles at proper time $\tau = 1$ fm/c compare well with hydrodynamical assumptions for initial energy density distributions.

Key words: ultra-relativistic heavy ion collisions, microscopic transport model, energy density, equilibration

PACS: 25.75.-q, 25.75.Nq, 24.10.Lx, 12.40.Nn

1 Introduction

Ultra-relativistic heavy ion collisions as performed within experiments at the Relativistic Heavy Ion Collider (RHIC) in Brookhaven offer a unique opportunity to study the nuclear phase diagram at high temperatures and densities [1]. For such extreme conditions the fundamental theory of strong interactions (Quantum Chromo Dynamics - QCD), i.e. lattice QCD calculations [2,3,4] predict a transition to a plasma of deconfined quarks and gluons (QGP). This state is believed to behave like a strongly coupled liquid rather than a free parton gas [5].

It is a generally accepted opinion that the preconditions for the phase transition to a QGP are readily fulfilled at RHIC energies. In the meantime exist

several experimental evidences that such a phase transition has indeed been seen [6,7,8,9].

The strongest theoretical argument comes from lattice QCD which predicts the phase transition at a critical temperature of around 170 MeV which corresponds to a critical energy density of around $0.7 \dots 1.3 \text{ GeV/fm}^3$ (depending on the number of degenerate quark flavours) at zero net baryon density [10,11]. Estimates from pseudorapidity distributions of charged particles and elliptic flow results from the PHOBOS Collaboration indicate that in central collisions at $\sqrt{s_{NN}} = 200 \text{ GeV}$ energy densities $\epsilon \geq 3 \text{ GeV/fm}^3$ are produced [7] when the system reaches approximate equilibrium. Such high energy densities, which are about twenty times the energy density inside nuclei and about six times the energy density inside nucleons, exceed clearly the values for the critical energy density predicted from lattice QCD. However, lattice calculations are performed for equilibrated matter and infinite systems. This rises questions for the size of the space-time volume in which a heavy ion collision exceeds the critical energy density and also the degree of equilibration which is reached inside this volume. Therefore the evolution and absolute magnitudes of the energy density within the first few fm/c after the collision are of particular interest.

Also the fact that the system enters the hydrodynamical regime at RHIC energies $\sqrt{s_{NN}} = 130 \div 200 \text{ GeV}$ is often interpreted as an evidence for a phase transition [12]. In contrast to SPS, at RHIC a simultaneous description of elliptic flow pattern as well as of low p_T ($p_T \lesssim 2 \text{ GeV}$) single particle spectra around mid-rapidity can be achieved within the hydrodynamics approach. This success has led to the conclusion that the created matter behaves like an *ideal fluid* with almost negligible viscosity [13,14] and that the time scale to reach such an locally equilibrated state is extremely short, i.e. less than 1 fm/c [15].

From an experimental point of view, it is almost impossible to extract information about initial pressure or energy densities and their equilibration times. Hydrodynamical calculations themselves provide only little insight in these questions since they are based on the assumption of local thermal equilibrium and short equilibration times. However, also hydrodynamics does not provide a perfect description of RHIC data. In particular, deviations of the hydrodynamical predictions for v_2 and v_4 from the measured elliptic flow were recently interpreted as a breakdown of the hydrodynamical picture and a hint towards incomplete equilibration [16]. In the hydrodynamics approach an ansatz for the early stage, i.e. at about 1 fm/c after the initial collision, is used as input for the evolution of the system. This requires to fix the initial energy density and net-baryon number density profiles. Usually for both distributions a boost-invariant distribution over a wide range of η_s , the so called space-time rapidity is chosen.

Transport models on the other hand, allow to study the dynamical evolution of thermodynamical properties of the colliding system from a microscopic point of view. String-cascade models of that type, e.g. UrQMD [17,18], HSD [19,20] or the quark-gluon string model (QGSM), do not contain an explicit phase transition to a deconfined partonic state but they can be used to study the preconditions for a possible phase transition and the results can be compared with the assumptions made by hydrodynamical approaches. The quark-gluon string model, applied in the present work and described in detail in Refs. [21,22,23,24,25] is a string model based on Gribov Regge Theory. The main assumption within these kind of (string-) models is that hadrons are produced as a result of excitation and decay of open strings with different quarks or diquarks at their ends. The QGSM provides a safe basis for the present investigations since it has been demonstrated to describe the elliptic flow bulk properties at SPS and in particular at RHIC energies reasonably well [26,27,28].

2 Evolution of energy density

In order to obtain an impression of the temporal evolution of the energy density ϵ we consider as two typical examples a central ($b = 0$ fm) and a semi-peripheral ($b = 8$ fm) Au+Au reaction at top RHIC energy of $\sqrt{s_{NN}} = 200$ GeV. In the present approach the energy density is locally determined in cells of 1 fm^3 volume through the scalar mass density of all formed and pre-formed hadrons inside these cells¹. All QGSM results are obtained from averages over 200 central reactions ($b = 0$ fm), respectively 600 semi-peripheral reactions ($b = 8$ fm). For simplicity, kinetic contributions to the energy density are neglected. Thus, the ϵ values presented in the following analysis have to be interpreted as lower limits of the total amount achieved in the collisions. To clarify this a bit more, let us consider a central collision at the very first instant when the two Lorentz contracted gold nuclei with a longitudinal size of ≈ 0.1 fm and a transverse area of $\approx 150 \text{ fm}^2$ overlap totally. This yields an energy density of $\approx 25 \text{ GeV}/\text{fm}^3$ in this approach.

Fig. 1 displays the time evolution of the local energy density ϵ in the x-z plane as a function of the system time t in the c.m. frame of the colliding nuclei. One should thereby keep in mind that the corresponding hypersurfaces where $\epsilon(\mathbf{x}, t = \text{const.})$ is evaluated are essentially different from hypersurfaces of proper time $\epsilon(\mathbf{x}, \tau = \text{const.})$ which are used to characterize the time evolution in hydrodynamics. The latter case will be discussed later on.

One immediately recognises in the contour plot of Fig. 1, that most particles

¹ Exceptions to this specification are appropriately indicated.

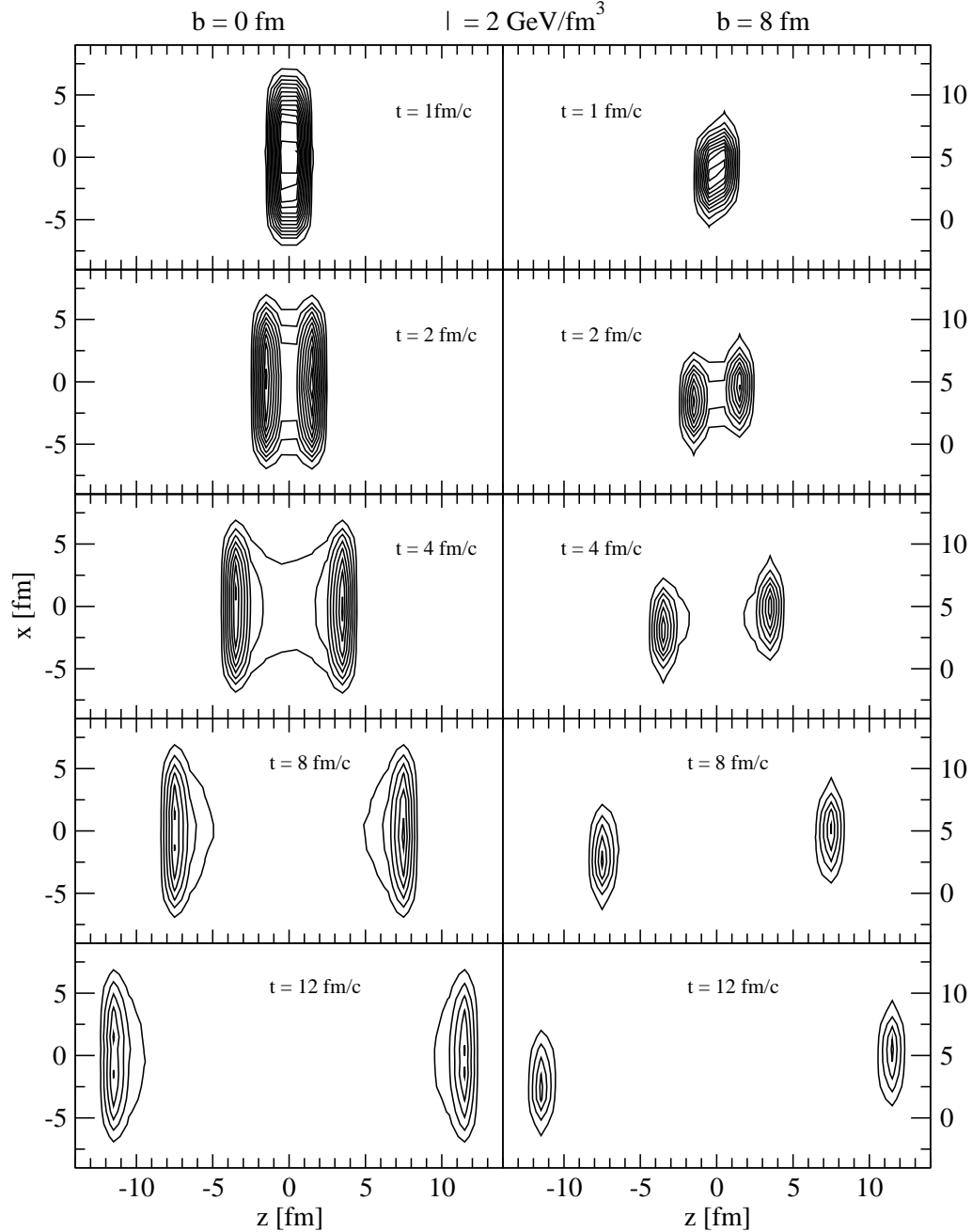


Fig. 1. Evolution of the energy density in the x - z plane for two different impact parameters, $b = 0$ fm (left) and $b = 8$ fm (right). Each line corresponds to an energy density interval of $2 \text{ GeV}/\text{fm}^3$.

do not stay in the central collision zone but rather form some kind of “shock waves”, i.e. two disks in the fragmentation regions occupied with large numbers of produced particles which propagate with high rapidities in front of the expanding system. As a result of that, the energy density in these zones stays at a high level for the whole time under consideration and decreases only slowly. Therefore most collisions happen within these zones while the center

of the volume between the two disks is rapidly thinning out of hadrons. After the first initial collisions energy densities of a few tens of GeV are achieved in the overlap zone of the central as well as semi-peripheral reaction.

To study the initial phase and the overlap zone more closely, we consider now the average energy density inside a larger volume of 64 fm^3 . For the central reaction we choose the central reaction zone, i.e. the most central cell given by $-2 \text{ fm} < x, y, z < 2 \text{ fm}$ and for the $b = 8 \text{ fm}$ case a volume shifted by 4 fm in x-direction, i.e. $2 \text{ fm} < x < 6 \text{ fm}$, $-2 \text{ fm} < y, z < 2 \text{ fm}$. Fig. 2 displays the time evolution of ϵ in the corresponding cells. One sees, that for the central collision a maximum energy density of around $15 \text{ GeV}/\text{fm}^3$ is reached while the semi-peripheral collision reaches a maximal ϵ of around $10 \text{ GeV}/\text{fm}^3$. Again, we want to emphasize that all particles are taken into account, i.e. first of all no rapidity cut is applied. The energy density stays almost constant

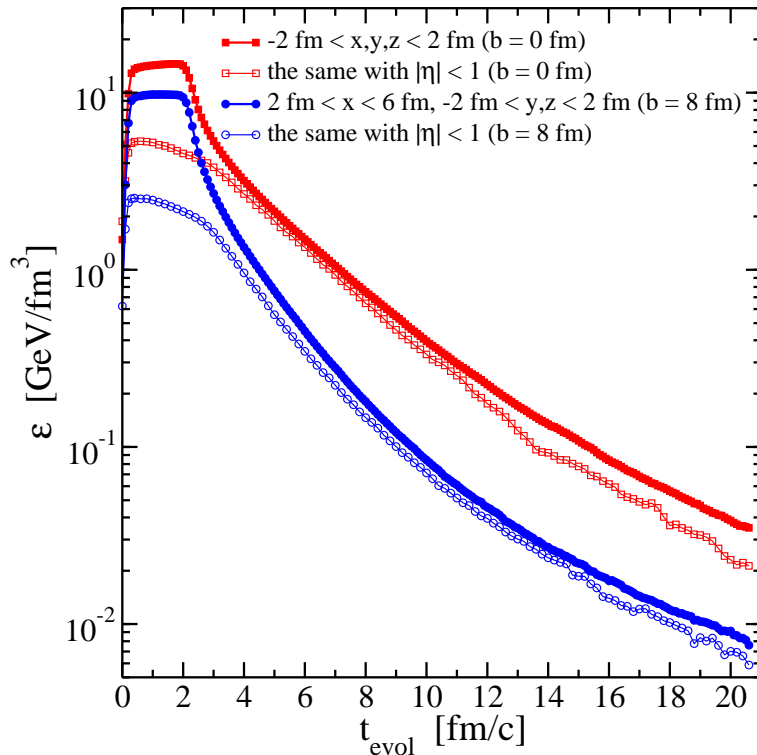


Fig. 2. Evolution of the energy density for a central cell in the overlap zone of the collision given by $-2 \text{ fm} < x, y, z < 2 \text{ fm}$ for $b = 0 \text{ fm}$ and $2 \text{ fm} < x < 6 \text{ fm}$, $-2 \text{ fm} < y, z < 2 \text{ fm}$ for $b = 8 \text{ fm}$. The curves with open symbols are the same but only for particles with a pseudorapidity of $|\eta| \leq 1$. See discussion in the text.

during the first $2 \text{ fm}/c$. It is even slightly increasing due to the ongoing particle production through scattering of projectile and target nucleons and the corresponding continuous energy deposit. As soon as the fastest particles start to leave the cell, what happens at around $t \approx 2 \text{ fm}/c$, ϵ is rapidly decreasing. This means that we obtain energy densities of $15 \text{ GeV}/\text{fm}^3$ in a space-time

volume of at least $\sim 130 \text{ fm}^4$ in the central collision and correspondingly about $10 \text{ GeV}/\text{fm}^3$ in the same volume for the semi-peripheral reaction. However, at that time the system is far from local equilibrium, as will be seen later on. It is stated in Ref. [7] that the value of the energy density for such a system, although well defined, may not be very interesting. The potentially more interesting quantity should be the energy density carried by particles which are closer to equilibrium conditions, wherefore the analysis in [7] was restricted to hadrons with pseudorapidities $|\eta| \leq 1$. To make a comparison between the estimates of the PHOBOS Collaboration and the QGSM results more transparent, two additional curves for the temporal evolution of ϵ with the same $|\eta| \leq 1$ restriction are depicted in Fig. 2. Here, energy densities in the order of $\geq 4 \text{ GeV fm}^{-3}$ in the central collisions and $\geq 2 \text{ GeV fm}^{-3}$ in the semi-peripheral reactions are obtained after $2 \text{ fm}/c$ time of evolution. These values are in nice agreement with the lower limit estimation of $\epsilon \geq 3 \text{ GeV fm}^{-3}$ produced in central Au+Au collisions at RHIC after $1 - 2 \text{ fm}/c$, as it is reported by the PHOBOS Collaboration [7]. Note, that also the QGSM results are lower limits of the produced energy densities as mentioned before. The actual densities could easily be significantly larger. Nevertheless, the parton-string cascade model is not able to equilibrate completely the system at such short time scales, as we will discuss later on.

As clearly seen from Fig. 1, the geometry of the colliding system is dominated by the leading particles which move practically on the light cone in beam (z) direction. In order to remove distortions from Lorentz contraction effects in a rapidly longitudinally expanding system one can introduce the so called space-time rapidity η_s . This is done by the introduction of cylindrical coordinates in t - and z -direction according to

$$(t, x, y, z) = (\tau \cosh \eta_s, x, y, \tau \sinh \eta_s) \quad (1)$$

with the longitudinal proper time $\tau = \sqrt{t^2 - z^2}$. The space-time rapidity is then given by the following expression:

$$\eta_s = \frac{1}{2} \ln \frac{t+z}{t-z} \quad . \quad (2)$$

The evolution of the energy density can now be displayed as a function of the boost-invariant variable η_s . Fig. 3 shows the energy density in the $x - \eta_s$ plane at the same time steps as have been used in Fig. 1. The y -coordinate is thereby restricted to the interval $0 < y < 1 \text{ fm}$. Also as a function of η_s the system has an energy density distribution with a nontrivial shape in the reaction plane. For the central collision, ϵ is rather Gaussian distributed in x -direction whereas it shows a characteristic double-peaked structure in η_s -direction, where the maxima follow the leading particles. This qualitative feature of the energy density distribution is practically maintained in the overlap

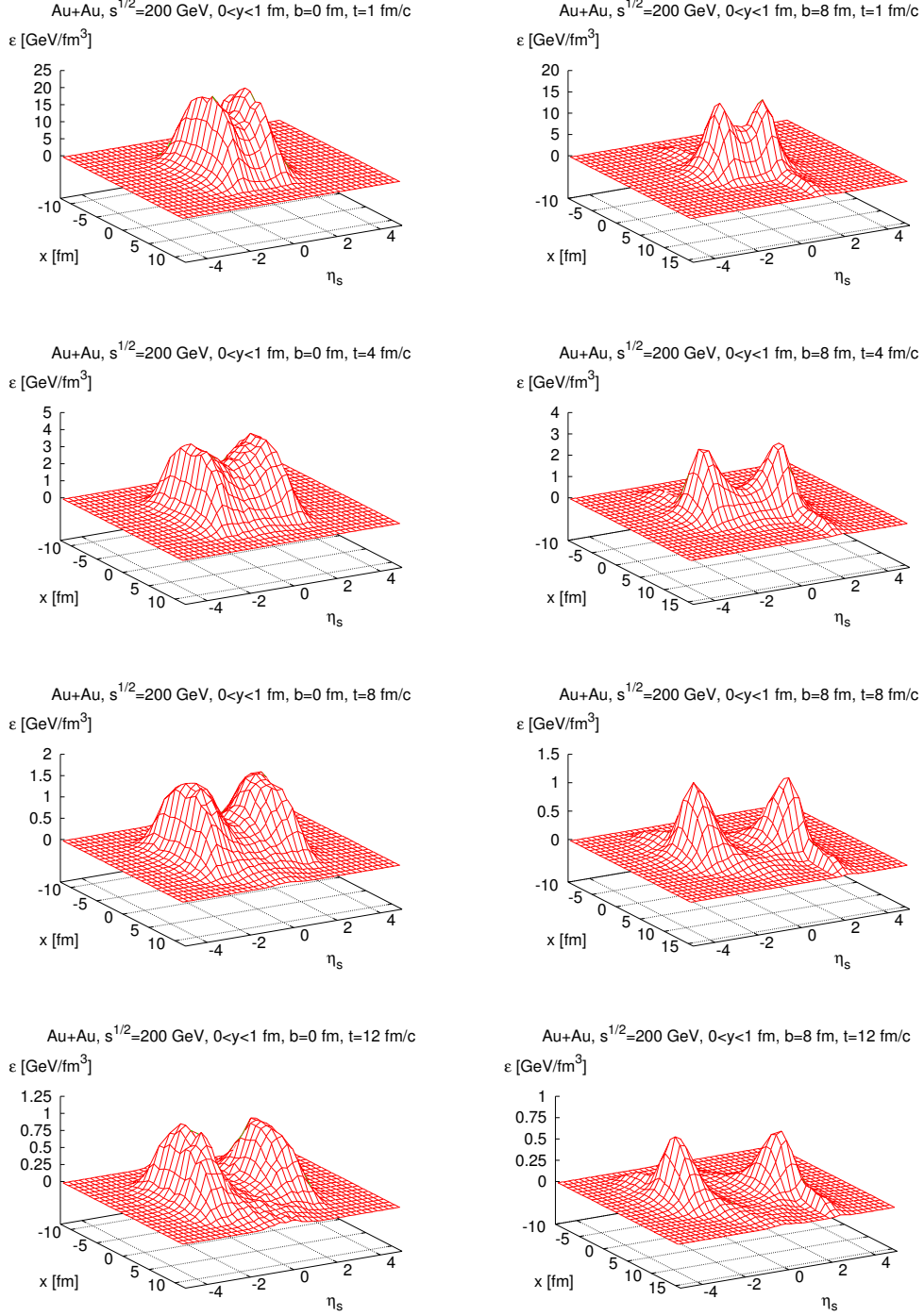


Fig. 3. Snapshots of the energy density ϵ in the $x - \eta_s$ plane at times $t = 1, 4, 8, 12$ fm/c. Note the different scales for ϵ .

zone of the semi-peripheral collision, albeit it is narrower distributed along the x -axis. Additionally, one clearly recognises the ϵ contributions of the spectators (“shoulders” at large $|x|$ and $|\eta_s|$) which propagate with about the same velocity as the high density bumps formed by the leading particles. Within the first

few fm/c of the expansion the central values are large, i.e. $\epsilon \approx 10 \div 15$ GeV/fm³ and the distributions are more compact. However, as already seen from Fig. 2, ϵ drops rapidly when the system expands. This decrease with increasing time is more pronounced in the central zone forming the “dip” than for the bumps following the leading particles. But also there the absolute values drop significantly and the peaks get washed out due to ongoing secondary collisions between the produced hadrons.

Complementary to the energy density in the reaction plane, the corresponding distributions of ϵ in the transversal (x - y) plane are depicted in Fig. 4. Here we consider only the central reaction with $b = 0$ fm. The contributions of the

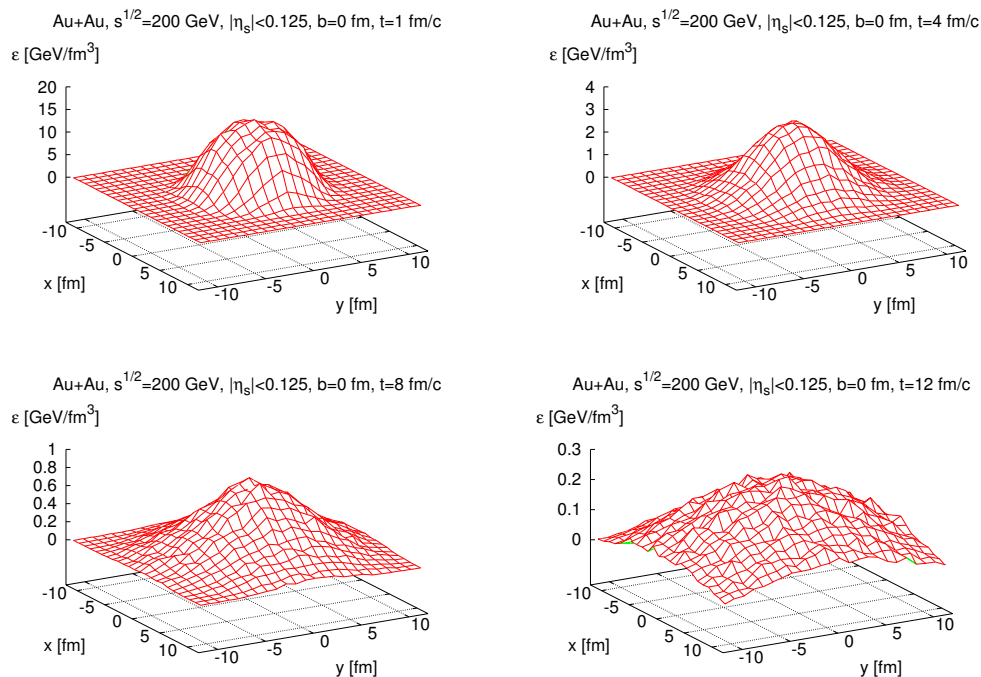


Fig. 4. Snapshots of the energy density in the transversal plane for a space-time rapidity slice of $|\eta_s| < 0.125$ obtained for a central ($b = 0$ fm) Au+Au collision at times $t = 1, 4, 8,$ and 12 fm/c.

leading particles are subtracted by restricting the space-time rapidity to the interval $|\eta_s| < 0.125$ in all the four time steps under consideration. The distributions look now more isotropic, i.e. Gaussian shaped in x - and y -direction, and are peaked at the origin of the transversal plane. As already seen from the previous figures, the peak value of ϵ reaches up to 15 GeV/fm³ for $t = 1$ fm/c. Although the energy density is rapidly decreasing in the transverse directions as well as in time, there exist definitely regions with values of ϵ within the first 8 fm/c, that are higher than the expected critical energy density for a phase transition to a deconfined phase.

Finally, the energy density ϵ is evaluated for the central reaction at constant

proper time $\tau = 1$ fm/c. The QGSM result is shown in Fig. 5. The depicted distributions can be directly compared with initial energy density distributions used in hydrodynamical calculations [29,30,31]. The ϵ distribution in the reac-

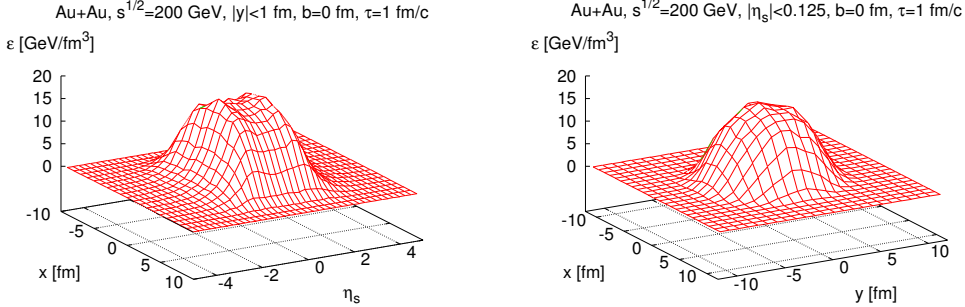


Fig. 5. Energy density of central Au+Au collisions in the reaction plane ($|y| < 1$ fm and $|x|, |\eta_s| \geq 0$) – left panel, and in the transversal plane ($|\eta_s| < 0.125$ and $|x|, |y| \geq 0$) – right panel, evaluated for constant longitudinal proper time $\tau = 1$ fm/c.

tion plane as obtained in the QGSM is rather similar to the initial energy densities investigated by Hirano et al. for Au+Au collisions at $\sqrt{s_{NN}} = 130$ GeV in a hydrodynamical model [29,30]. The distribution is nearly flat in the region $|\eta_s| \leq 1.0$ and connects to vacuum as a kind of Gaussian function sharply decreasing in the forward and backward space-time rapidity regions. The di-

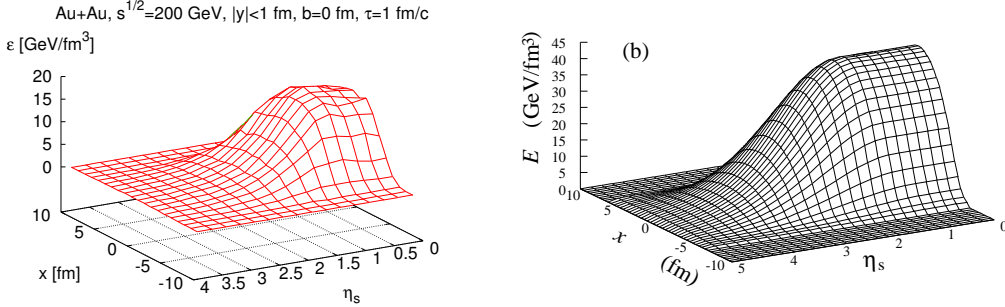


Fig. 6. Energy density in the reaction plane of central collisions obtained in the QGSM for $\tau = 1$ fm/c – left panel (the same as on the left of Fig. 5 but rescaled), and initial distribution used in hydrodynamical calculations by Hirano et al. – right panel. The figure on the right is taken from Ref. [29].

rect comparison of the microscopically determined density profile on the one side and a hydrodynamical model assumption from Ref. [29] on the other side – illustrated in Fig. 6 – exemplifies this fact. Also in the transversal plane the shape and order of magnitude of ϵ at $\tau = 1$ fm/c is supported by a hydrodynamical calculation of Ref. [31], where the NeXuS event generator [32] has been used to determine the initial conditions for central Au+Au collisions at $\sqrt{s_{NN}} = 130$ GeV. There it has been shown that fluctuations of the

initial conditions produced by a microscopic model and used as input for hydrodynamical calculations are important and lead to discrepancies for some observables. Together with our findings for the averaged distributions of energy density the assumption of smooth and symmetric initial conditions seems to be a rather rough one.

3 Local equilibration

As one can expect from the energy density distributions of Fig. 1, global equilibrium cannot be reached; the distributions of particles are far from being isotropic for all time steps under consideration. But when one looks in more detail, some cells could reach local equilibrium. In order to measure the degree of kinetic equilibration for a given cell, the pressure components for the x-, y- and z-direction are calculated [33]. The diagonal elements of the pressure tensor in a cell according to the virial theorem are given by [34]

$$P_{\{x,y,z\}} = \frac{1}{3V} \sum_i \frac{p_{i,\{x,y,z\}}^2}{\sqrt{m_i^2 + p_{i,x}^2 + p_{i,y}^2 + p_{i,z}^2}}, \quad (3)$$

where V is the volume of the cell, m_i is the mass and $p_{i\{x,y,z\}}$ are the momentum components of hadron i . The sum runs over all hadrons in the corresponding cell. The pressure is locally evaluated, therefore a Lorentz transformation with the average velocity in the x-, y- and z-direction is applied before taking the sum. The requirement of isotropic velocity distributions, i.e. kinetic equilibrium, is closely related to the requirement of the pressure isotropy, which would imply $P_x = P_y = P_z$. Therefore, the equilibration ratio R_{LE} as defined by

$$R_{LE} = \frac{1}{2} \frac{P_x + P_y}{P_z} \quad (4)$$

is evaluated for each cell as a measure of local equilibration. Local equilibrium in the corresponding cell is then characterized by $R_{LE} \rightarrow 1$.

First of all, the equilibration process is studied for the central cell of the collision, given by $-2 \text{ fm} < x, y, z < 2 \text{ fm}$ for $b = 0 \text{ fm}$ and $2 \text{ fm} < x < 6 \text{ fm}$, $-2 \text{ fm} < y, z < 2 \text{ fm}$ for $b = 8 \text{ fm}$, by looking at the pressure for all three directions. Fig. 7 shows the pressure components as defined in Eq. (3) for the central and the semi-peripheral collisions. In both reactions the longitudinal pressure is clearly dominating the very early evolution of the system while the transversal pressure components in x- and y-direction are nearly equal. At $t \approx 2 \text{ fm}/c$ the longitudinal pressure starts to decrease drastically and

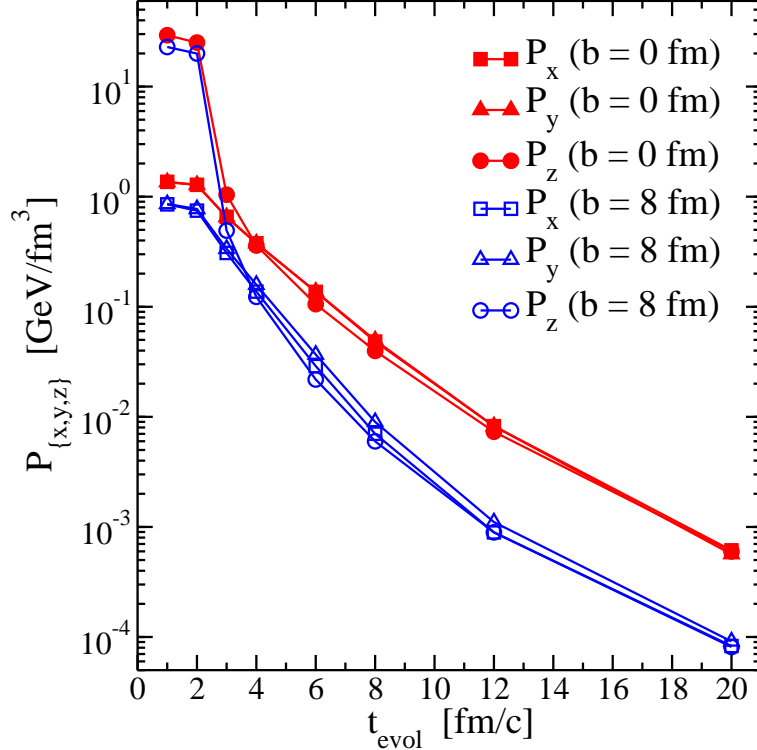


Fig. 7. Pressure components in x-, y- and z-direction in the central cell of the overlap zone of the colliding gold nuclei with $b = 0$ fm and $b = 8$ fm, respectively.

reaches a level close to the transversal pressure after ≈ 4 fm/c time of evolution. Thereafter all the three corresponding pressure components decrease with similar slopes. Nevertheless, the pressure isotropy is not yet achieved because deviations up to 30 – 50 % between the longitudinal and transversal components occur during the next 8 fm/c. Following the discussion in [33], one can call this a pre-equilibrium stage. It sets in very quickly for both, the central and the semi-peripheral collision, whereas the dynamics of the kinetic equilibration process during the pre-equilibrium stage is somewhat different for both reactions.

This difference in the degree of equilibration is clearly seen, when one additionally looks at the equilibration ratio R_{LE} defined in Eq. 4. Fig. 8 depicts R_{LE} in the central cell of the overlap zone for central and semi-peripheral Au+Au collisions. Again, the pre-equilibrium stage with $R_{LE} \approx 1$ is reached for central collisions after 4 fm/c corresponding to a time when the high density areas as seen in Fig. 1 and Fig. 2 have completely passed through the central cell. Within these high density areas the longitudinal pressure is clearly dominating and therefore no equilibrium can be reached. During the next few fm/c the transverse pressure components are slightly dominating the expansion; the equilibration ratio tends to be greater than one. But it decreases already after ≈ 6 fm/c time of evolution and – as the cell is losing more and more particles – approaches almost local equilibrium after 12 – 15 fm/c. The transverse pres-

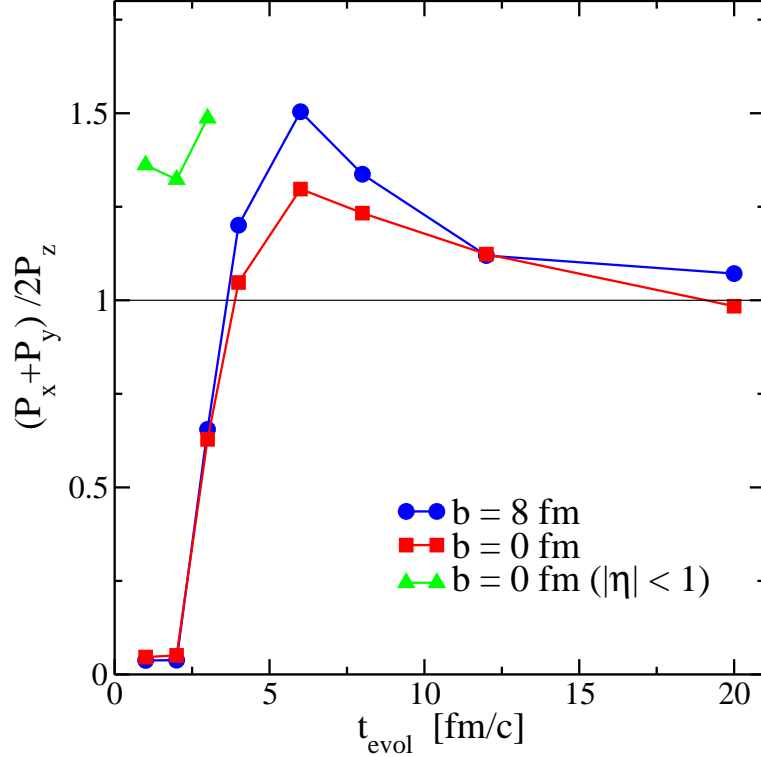


Fig. 8. Degree of equilibration as defined by the equilibration ratio R_{LE} in the central cell of the overlap zone for Au+Au collisions at $\sqrt{s_{NN}} = 200$ GeV with impact parameters $b = 0$ fm and $b = 8$ fm. The triangles indicate the equilibration ratio of particles with pseudorapidities $|\eta| \leq 1$ only, produced within the first 3 fm/c of the central collisions (see detailed discussion below).

sure components P_x and P_y are nearly equal to each other during this stage, what reflects the symmetry of the collision zone in the transverse plane.

In case of the semi-peripheral collision with an impact parameter of 8 fm local equilibrium seems not to be reached in the cell corresponding to the overlap zone of the collision after 15 fm/c, but nevertheless R_{LE} gets at least very close to unity. After the high density areas passed through the cell, the transverse pressure is clearly dominating the next few fm/c of the pre-equilibrium stage – stronger than in the central collision, but in contrast to the central reaction it is itself not equilibrated. As can be seen in Fig. 7, the y-component of the pressure tends to be greater (up to 30%) than the x-component. This asymmetry arises due to the elliptical overlap of the colliding nuclei and reflects the smaller pressure gradients in the y-direction, which, in the hydrodynamical picture, is responsible for the build-up of elliptic flow [35].

The question, to what extent the produced matter reaches thermalization and how fast this may be achieved, is still open. In Ref. [16] it was shown that the linear rise of elliptic flow, in particular v_2/ε with ε being the eccentricity of the spatial overlap of the colliding nuclei at RHIC, with the density gives

rise to the conclusion of a density dependence and hence to a small number of collisions per particle. Thermalization could therefore not be reached so fast. Our findings of equilibration at around $t \approx 15$ fm/c together with the elliptic flow results and their time evolution obtained in the QGSM [28,36,37] support this picture and contradict quasi the usual hydrodynamical assumptions of fast thermal equilibration.

However, as can be seen in Fig. 8 a certain fraction of the produced particles, i.e. hadrons with pseudorapidities $|\eta| \leq 1$, is closer to local equilibrium even at times $t \approx 1$ fm/c. In between the two currents of matter of the target and projectile fragmentation regions, which make up $\approx 2/3$ of the energy density, this fraction provides a dense and roughly equilibrated local surrounding even at very early times of central heavy ion collisions. Thus we find energy densities of about $4 - 5$ GeV fm $^{-3}$ in central Au+Au reactions at $\sqrt{s_{NN}} = 200$ GeV for matter which can be considered to be at least in a pre-equilibrium stage already at $1 - 2$ fm/c. The preconditions for a phase transition, i.e. energy densities $\epsilon > \epsilon_{\text{crit}} \simeq 1$ GeV fm $^{-3}$, are given for a duration of ≈ 8 fm/c in a space-time volume of about 500 fm 4 .

Finally, the degree of local equilibration and its time evolution is evaluated in the whole reaction ($x - z$) plane for the central and semi-peripheral Au+Au collisions. All the results depicted in Fig. 9 for the three time steps $t = 4, 8,$ and 12 fm/c show a characteristic saddle structure, which is more smoothly and faster developed in the central than in the semi-peripheral reaction. For the x-direction the equilibration ratio R_{LE} always has a minimum in the overlap zone whereas it reaches here the maximum as a function of the longitudinal coordinate z . The high density areas in front of the expanding system, in other words at large values of z , never reach local equilibrium; only in the aftermath of the pass-through the inner cells tend towards kinetic equilibration indicated by $R_{LE} \approx 1$. In the center of the collision the transverse pressure is dominating at all times, therefore is $R_{LE} > 1$. But towards higher densities in the z -direction the longitudinal, i.e. z -component of the pressure is increasing and therefore supplying more equilibrated zones filled with outward moving particles. Since the most collisions naturally happen within the high density areas, it is important to notice that the most secondary particle interactions take place in a non-equilibrated surrounding.

Closing the discussion, it should be mentioned that string-cascade models provide most likely an upper limit for relaxation times towards local equilibrium. This is not only due to the fact that models of this type do not contain a phase transition to partonic degrees of freedom which are expected to equilibrate much faster. Standard string-cascade models violate detailed balance since particle production through string decays leads to processes $2 \rightarrow N$ with two initial and N final state hadrons. However, corresponding backward processes $N \rightarrow 2$ are not included. This approximation is usually justified by

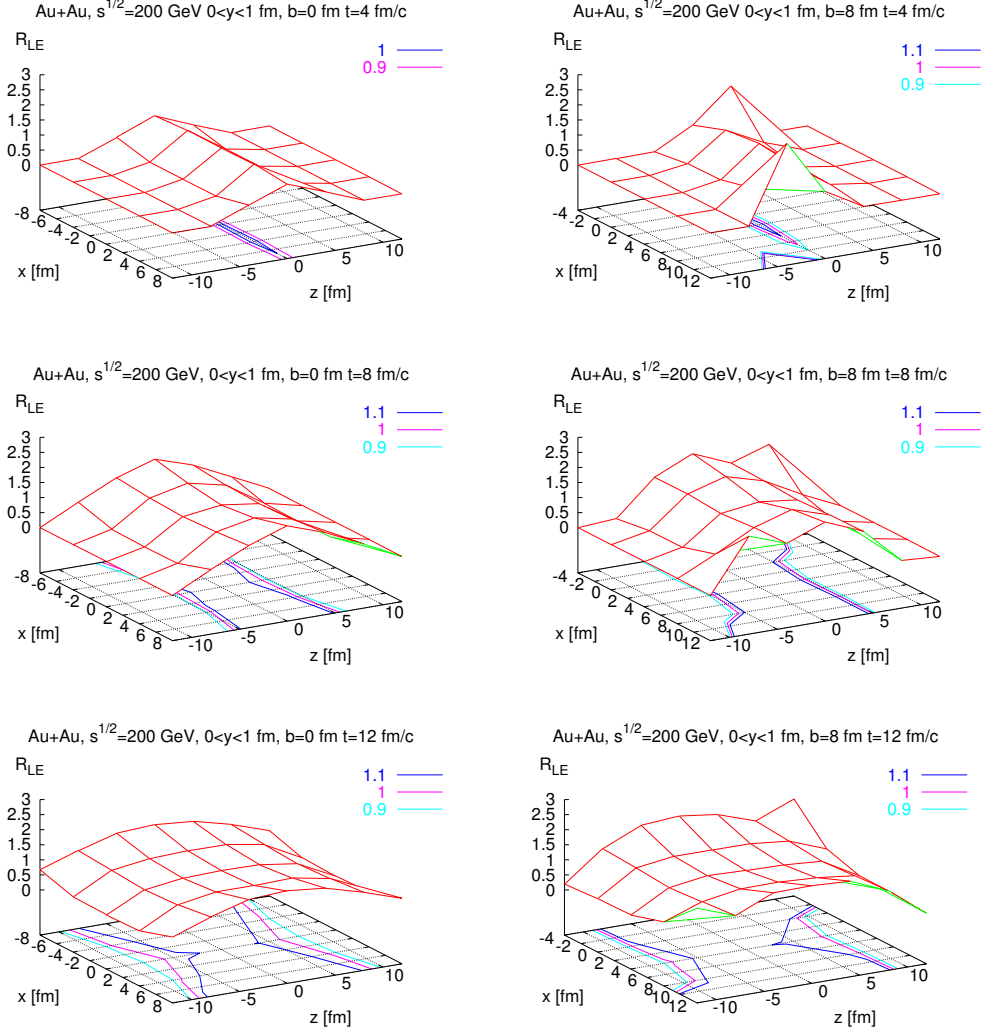


Fig. 9. Snapshots of the equilibration ratio R_{LE} in the overall x - z plane after $t = 4, 8,$ and 12 fm/c time of evolution. The distributions on the left are for collisions with $b = 0$ fm, and on the right for collisions with $b = 8$ fm.

the assumption that many-body scattering processes $N \rightarrow X$ play a minor role in open, fast expanding systems. However, when high particle densities are achieved such processes can become relevant, e.g. for the production of rare hadron species [38]. Many-body processes, such as string or hadron fusion and recombination, lead naturally to shorter equilibration times, as has e.g. been demonstrated in [39] for the gluonic sector. In very dense states of matter it is expected that interactions among strings, before they fragment into hadrons, are able to accelerate the equilibration process in microscopic string models. Possible concepts in this context are the before mentioned string fusion, the formation of string clusters, and eventually percolation of strings, which have been considered in several string-cascade models [40,41,42,43,44]. Effectively, such processes describe reactions of $2n$ ($n \geq 2$) initial particles going to N final state hadrons. Nevertheless, detailed balance is still violated. But fu-

ture studies should be dedicated to the question how far these multi-string processes are able to reduce quantitatively the relaxation times towards local equilibrium.

4 Summary and conclusions

In this survey, we have analysed several aspects of the collision dynamics in central and semi-peripheral Au+Au reactions at the highest RHIC center of mass energy of $\sqrt{s_{NN}} = 200$ GeV within the microscopic quark-gluon string model (QGSM), which is based on the colour exchange mechanism for string formation.

The first major topic was dedicated to the time evolution of the local energy density ϵ . Maximum energy densities of around 15 GeV/fm³ for the central collisions and around 10 GeV/fm³ in semi-peripheral reactions are reached in the overlap zone after the first initial hadron collisions. The energy density stays almost constant in the central cell during the first 2 fm/c time of evolution. The value of ϵ in this cell is rapidly decreasing as soon as the fastest particles start to leave the cell. This happens at around $t \approx 2$ fm/c. The corresponding ϵ distributions in the x-z plane as a function of the system time t in the c.m. frame of the colliding nuclei reveal, that most particles do not stay in the central collision zone but form two disks in the fragmentation regions occupied with large numbers of produced particles which travel practically on the light cone in beam (z) direction. Also as a function of the boost-invariant space-time rapidity η_s , the system has an energy density distribution with a nontrivial shape in the reaction plane, i.e. a characteristic double-peaked structure in η_s -direction which is maintained in the central and also in the semi-peripheral collisions. Complementary to the energy density in the reaction plane, the corresponding distributions of ϵ in the transversal plane and additionally at constant proper time $\tau = 1$ fm/c were studied (only for the central reaction). The QGSM results of the latter distributions compare well with hydrodynamical assumptions for initial energy density profiles [29,30,31]. These are similar in shape as well as in the order of magnitude. Nevertheless, the absolute values of ϵ drop rapidly when the system expands and the peaks get significantly washed out due to ongoing secondary collisions between the produced particles. But we want to emphasize that, although ϵ is rapidly decreasing in the transverse directions as well as in time, there definitely exist regions with local energy densities higher than the expected critical energy density for the QCD phase transition within the first 8 fm/c.

However, at that time the system is not completely in local equilibrium, as it was elaborated in the second major topic. There the question whether and how fast the produced particles in ultra-relativistic Au+Au collisions equi-

brate has been studied. It was shown that in both reactions, i.e. central and semi-peripheral ones, the longitudinal pressure is clearly dominating within the first 2 fm/c. After the fast particles have left the central cell, all the three pressure components converge to each other. The next 8 fm/c the transverse pressure is slightly stronger, not allowing the system to reach full local equilibrium but entering some kind of pre-equilibrium stage. As the central cell of the overlap zone is loosing more and more particles, it approaches almost local equilibrium after 12 – 15 fm/c in the central collisions and 15 – 20 fm/c in case of the semi-peripheral reactions. Finally, the degree of local equilibration characterized by R_{LE} and its time evolution in the whole reaction ($x - z$) plane shows in the central and semi-peripheral Au+Au collisions for all considered time steps a characteristic saddle structure, which indicates that the high density areas in front of the expanding system are far away from local equilibrium. Only the inner cells tend towards kinetic equilibration. Since the most secondary collisions happen within these high density areas, the most particle interactions take place in a non-equilibrated surrounding. Global equilibrium is not reached at all – the global particle distributions are far from being isotropic for all time steps under consideration.

As it was already mentioned, the question to what extent the produced matter reaches thermalization and how fast this may be achieved in the experiment is still open. Our findings of almost full local equilibration at around $t \approx 15$ fm/c together with the elliptic flow results and their time evolution obtained in the QGSM [28,36,37] support the idea that fast thermal equilibration is not necessary to produce large elliptic flow, what contradicts somehow the usual hydrodynamical assumptions. Nevertheless, a pre-equilibrium stage with energy densities well above the critical energy density is already achieved at early time scales. This means that the preconditions for a phase transition can be found within the string-cascade approach which, due to the lack of multi-string and/or multi-particle fusion processes, provides an upper limit for the equilibration times.

In this context, it is also important to stress, that all calculations are performed by averaging over 200 and 600 events for central and semi-peripheral reactions respectively. For a single collision event the energy density as well as local equilibrium is subject to strong fluctuations. It is not a priori clear to what extent these fluctuations may contribute to the final observables, as has been pointed out in Ref. [31]. This question together with a more detailed understanding of the freeze-out scenario for the hadron production and the influence of multi-string/particle reactions on equilibration deserves further investigations.

Acknowledgments

This work was supported by the Bundesministerium für Bildung und Forschung (BMBF) under contract 06TÜ986.

References

- [1] Quark Matter 2004, *J. Phys. G* 30 (2004) 1.
- [2] Z. Fodor, S. D. Katz, K. K. Szabo, *Phys. Lett. B* 568 (2003) 73.
- [3] C. R. Allton, S. Ejiri, S. J. Hands, O. Kaczmarek, F. Karsch, E. Laermann, C. Schmidt, *Phys. Rev. D* 68 (2003) 014507.
- [4] P. de Forcrand, O. Philipsen, *Nucl. Phys. B* 673 (2003) 170.
- [5] E. Shuryak, *Prog. Part. Nucl. Phys.* 53 (2004) 273.
- [6] I. Arsene et al. [BRAHMS Collaboration], *Nucl. Phys. A* 757 (2005) 1.
- [7] B. B. Back et al. [PHOBOS Collaboration], *Nucl. Phys. A* 757 (2005) 28.
- [8] J. Adams et al. [STAR Collaboration], *Nucl. Phys. A* 757 (2005) 102.
- [9] K. Adcox et al. [PHENIX Collaboration], *Nucl. Phys. A* 757 (2005) 184.
- [10] F. Karsch, E. Laermann, arXiv:hep-lat/0305025, in: R. C. Hwa (ed.) et al., *Quark gluon plasma III*, World Scientific (Singapore), 1.
- [11] E. Laermann, O. Philipsen, *Ann. Rev. Nucl. Part. Sci.* 53 (2003) 163.
- [12] C. M. Hung, E. V. Shuryak, *Phys. Rev. Lett.* 75 (1995) 4003.
- [13] M. Gyulassy, L. McLerran, *Nucl. Phys. A* 750 (2005) 30.
- [14] E. V. Shuryak, *Nucl. Phys. A* 750 (2005) 64.
- [15] P. F. Kolb, U. W. Heinz, arXiv:nucl-th/0305084, in: R. C. Hwa (ed.) et al., *Quark Gluon Plasma III*, World Scientific (Singapore), 634.
- [16] R. S. Bhalerao, J. P. Blaizot, N. Borghini, J. Y. Ollitrault, *Phys. Lett. B* 627 (2005) 49.
- [17] S. A. Bass et al., *Prog. Part. Nucl. Phys.* 41 (1998) 225.
- [18] M. Bleicher et al., *J. Phys. G* 25 (1999) 1859.
- [19] J. Geiss, W. Cassing, C. Greiner, *Nucl. Phys. A* 644 (1998) 107.
- [20] W. Cassing, E. L. Bratkovskaya, *Phys. Rept.* 308 (1999) 65.
- [21] A. B. Kaidalov, *Phys. Lett. B* 116 (1982) 459.

- [22] A. B. Kaidalov, K. A. Ter-Martirosian, *Phys. Lett. B* 117 (1982) 247.
- [23] N. S. Amelin, L. V. Bravina, *Sov. J. Nucl. Phys.* 51 (1990) 133.
- [24] N. S. Amelin, K. K. Gudima, V. D. Toneev, *Sov. J. Nucl. Phys.* 51 (1990) 327.
- [25] N. S. Amelin, L. V. Bravina, L. P. Csernai, V. D. Toneev, K. K. Gudima, S. Y. Sivoklov, *Phys. Rev. C* 47 (1993) 2299.
- [26] E. E. Zabrodin, C. Fuchs, L. V. Bravina, A. Faessler, *Phys. Lett. B* 508 (2001) 184.
- [27] E. E. Zabrodin, C. Fuchs, L. V. Bravina, A. Faessler, *Phys. Rev. C* 63 (2001) 034902.
- [28] G. Bureau, J. Bleibel, C. Fuchs, A. Faessler, L. V. Bravina, E. E. Zabrodin, *Phys. Rev. C* 71 (2005) 054905.
- [29] T. Hirano, *Phys. Rev. C* 65 (2002) 011901.
- [30] K. Morita, S. Muroya, C. Nonaka, T. Hirano, *Phys. Rev. C* 66 (2002) 054904.
- [31] Y. Hama, T. Kodama and O. Socolowski Jr., *Braz. J. Phys.* 35 (2005) 24.
- [32] H. J. Drescher, S. Ostapchenko, T. Pierog, K. Werner, *Phys. Rev. C* 65 (2002) 054902.
- [33] L. V. Bravina et al., *Phys. Rev. C* 60 (1999) 024904.
- [34] M. Berenguer, C. Hartnack, G. Peilert, H. Stoecker, W. Greiner, J. Aichelin, A. Rosenhauer, *J. Phys. G* 18 (1992) 655.
- [35] P. Huovinen, arXiv:nucl-th/0305064, in: R. C. Hwa (ed.) et al., *Quark Gluon Plasma III*, World Scientific (Singapore), 600.
- [36] L. Bravina, K. Tywoniuk, E. Zabrodin, G. Bureau, J. Bleibel, C. Fuchs, A. Faessler, *Phys. Lett. B* 631 (2005) 109.
- [37] E. E. Zabrodin, L. V. Bravina, G. Bureau, J. Bleibel, C. Fuchs, A. Faessler, *J. Phys. G* 31 (2005) S995.
- [38] R. Rapp, E. V. Shuryak, *Phys. Rev. Lett.* 86 (2001) 2980.
- [39] Z. Xu, C. Greiner, *Phys. Rev. C* 71 (2005) 064901.
- [40] H. Sorge, *Phys. Rev. C* 52 (1995) 3291.
- [41] S. E. Vance, *J. Phys. G* 27 (2001) 603.
- [42] E. L. Bratkovskaya et al., *Phys. Rev. C* 69 (2004) 054907.
- [43] N. S. Amelin, N. Armesto, C. Pajares, D. Sousa, *Eur. Phys. J. C* 22 (2001) 149.
- [44] C. Pajares, *Eur. Phys. J. C* 43 (2005) 9.